Global changes in the connectome in autism spectrum disorders

Caspar J. Goch[a⋆], Basak Oztan[b⋆], Bram Stieltjes[c], Romy Henze[c,d], Jan Hering[a], Luise Poustka[e], Hans-Peter Meinzer[a], Bülent Yener[b] and Klaus H. Maier-Hein[a,c]

[a]German Cancer Research Center, Medical and Biological Informatics, Heidelberg, Germany;
[b]Rensselar Polytechnic Institute, Computer Science Department, Troy, New York, United States of America;
[c]German Cancer Research Center, Quantitative Imaging-based Disease Characterization, Heidelberg, Germany;
[d]Heidelberg University Hospital, Child and Adolescent Psychiatry, Section Disorders of Personality Development, Heidelberg, Germany;
[e]Department of Child and Adolescent Psychiatry and Psychotherapy, Central Institute of Mental Health, Mannheim, Germany
⋆ These authors contributed equally to this work.

Abstract. There is an increasing interest in connectomics as means to characterize the brain both in healthy controls and in disease. Connectomics strongly relies on graph theory to derive quantitative network related parameters from data. So far only a limited range of possible parameters have been explored in the literature. In this work, we utilize a broad range of global statistic measures combined with supervised machine learning and apply it to a group of 16 children with autism spectrum disorders (ASD) and 16 typically developed (TD) children, which have been matched for age, gender and IQ. We demonstrate that 86.7% accuracy is achieved in distinguishing between ASD patients and the TD control using highly discriminative graph features in a supervised machine learning setting.

Keywords: connectomics, network analysis, diffusion imaging, autism, classification

1 Introduction

The past decades have seen an increasing interest in using diffusion weighted imaging to examine the way the human brain is connected [1]. Differences in these connections have been found for many mental illnesses, e.g. autism spectrum disorders (ASD) [2]. These techniques have mainly been used to look at the integrity of single tracts [3] or a few global measures of the connectome, especially small-worldness and the clustering coefficient [4]. A few recent studies also looked at local changes in different brain areas, especially those related to speech [5, 6]. A disadvantage of these approaches is the need for anatomical knowledge about

the areas of interest and the lack of global information. Therefore, changes not localized in these specific areas are typically overlooked.

Recent studies focused on a limited number of measures to characterize the changes induced by ASD in connectome. However, the understanding and diagnosis of ASD can be improved upon a comprehensive evaluation of the connectome topology with a large number of network features at global scale. Global scale graph features are shown to successfully characterize structure-function relationships in various biological systems. Specifically, in histopathological image analysis and tissue modeling applications, *cell-graphs* are utilized for the computer-aided diagnosis of brain, breast, and bone cancers [7–10] and also for the modeling of stem cells [11], cell-mediated collagen remodeling [12], and salivary gland branching morphogenesis [13]. In this paper, we extend quantitative connectomics by investigating the roles of global graph features in capturing ASD induced changes. We demonstrate that support vector machines based supervised learning achieves 86.7% accuracy in classifying the ASD and TD connectomes.

2 Materials and Methods

Data Acquisition: Evaluation was performed on a group of 18 right-handed children (16 male and 2 female) with a mean (standard deviation) chronological age of 9.7 (2.1) with a diagnosis of Asperger Syndrome or High Functioning Autism. The control group of 18 typically developed children of age 9.7 (1.9) was matched for age, sex and IQ. Data acquisition was done using a 1.5 T scanner (Siemens Avanto). T1 images for parcellation were taken with the following settings: MPRAGE TR/TE/TI/α = 1.9 s/4 ms/1.1 s/8 °, FOV = 256 × 256 mm^2, matrix = 256 × 256, scan time 6 min). Diffusion weighted imaging was performed using single shot EPI with a dual bipolar diffusion gradient and a double spin echo for reduction of eddy currents with the following parameters: TR/TE 4700/78, FOV 192 mm, data matrix of 96 × 96 yielding an in-plane resolution of 2.0 mm, 50 axial slices with a thickness of 2.0 mm and no gap, with six gradient directions (b=1000 s/mm^2) and a b=0 image. This scheme was repeated 15 times.

Preprocessing and Fiber Tracking: The entire image processing pipeline is depicted in Fig. 1. The T1 weighted image was used to create a parcellation of the brain using freesurfer [14] as well as a binary mask of the brain. DWI data was motion and eddy-current corrected using FSL [15]. Q-ball images were then generated using solid angle reconstruction as provided by MITK [16]. Fiber tractography was performed on the q-ball images using the global tractography approach as presented by Neher et al. [17] using the brain mask to restrict the search space for possible fibers. To evaluate the robustness of our chosen tractography algorithm and the influence of the probabilistic tracking on our results we did four independent trackings for each patient. The same settings were used for each tracking: 10^8 iterations, particle length of 3.7 mm, particle width of 0.1 mm, particle weight of 0.0015, start temperature of 0.1, end temperature of

0.001, energy balance of 0, minimal fiber length of 20 mm and curvature threshold of 45°. Two patients and two controls were excluded due to heavy image artifacts and a resulting failure of the processing pipeline.

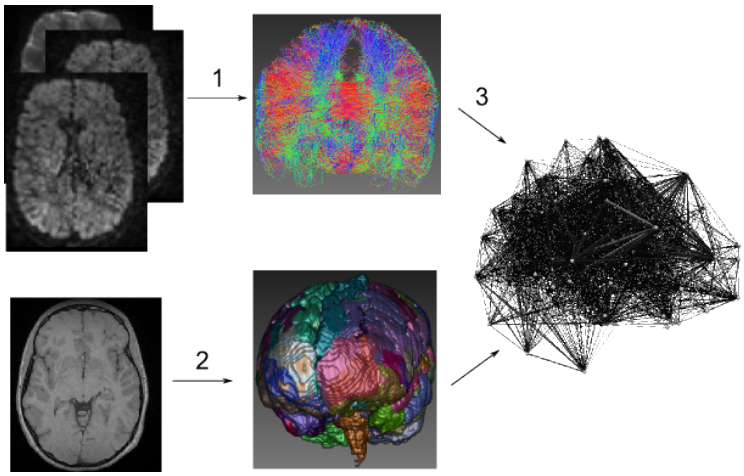

Fig. 1. Preprocessing pipeline. 1. Diffusion images are used to create a fiber image. 2. The anatomical MR image is used to create a parcellation of the brain. 3. The parcellation and the fiber image are used to create a network.

Network Generation: Connectivity matrices were created from the tractography result and the parcellation. DWI data and T1 images were registered using ANTs[1] for affine registration. Each label of the freesurfer segmentation was represented by one node if at least one fiber originated or ended within it. Two nodes were linked by an edge if at least one fiber connected the corresponding volumes. If a fiber could not be assigned two different non-white-matter labels it was disregarded. After network creation edges between nodes were eliminated if they represented less than N fibers to remove connections induced by noise. For this purpose, we performed a parameter search where we varied N between 14 and 30 with steps equal to 1 and select the value that yield the highest classification accuracy. Our analysis indicated $N = 26$ corresponded to the best classification performance.

Extraction of Connectome Features: We extracted 32 features for each patient's connectome. These features quantify the compactness, clustering, and spatial uniformity of the hypothesized connections within the brain. Graph features and their explanations are given in Table 1.

[1] http://www.picsl.upenn.edu/ANTS/

Table 1. Extracted graph features and their descriptions.

Feature Name	Description
Number of Nodes	Number of regions in brain
Number of Edges	Number of hypothesized communications
Average Degree	Number of edges per node
Clustering Coefficient C	Ratio of total number of edges among the neighbors of the node to the total number of edges that can exist among the neighbors of the node per node
Clustering Coefficient D	The average of the ratio of the links a node's neighbors have in between to the total number that can possibly exist
Clustering Coefficient E	Ratio of total number of edges among the neighbors of the node to the total number of edges that can exist among the neighbors of the node per node excluding the isolated nodes
Average Eccentricity	Average of node eccentricities, where the eccentricity of a node is the maximum shortest path length from the node to any other node in the graph
Diameter	Maximum of node eccentricities
Radius	Minimum of node eccentricities
Average Path Length	Average distance between the nodes of a graph, where the distance between two nodes is the number of edges in the shortest path that connects them
Average Betweenness	Average of node betweenness, where the betweenness of a node is the number of shortest paths from all nodes to all others that pass through that node
Giant Connected Component Ratio	Ratio between the number of nodes in the largest connected component in the graph and total the number of nodes
Number of Connected Components	Number of clusters in the graph excluding the isolated nodes
Average Connected Component Size	Number of nodes per connected component
Percentage of Isolated Points	Percentage of the isolated nodes in the graph, where an isolated node has a degree of 0
Percentage of End Points	Percentage of the end nodes in the graph, where an end node has a degree of 1
Number of Central Points	Number of nodes within the graph whose eccentricity is equal to the graph radius
Percentage of Central Points	Percentage of nodes within the graph whose eccentricity is equal to the graph radius
Spectral Radius	Largest valued eigenvalue of adjacency matrix
Second Largest	Second largest values eigenvalue of adjacency matrix
Adjacency Trace	Sum of the eigenvalues of adjacency matrix
Adjacency Energy	Sum of the squares of eigenvalues of adjacency matrix
Spectral Gap	Number of 0 valued eigenvalues of adjacency matrix
Laplacian Trace	Sum of the eigenvalues of laplacian matrix
Laplacian Energy	Sum of the squares of eigenvalues of laplacian matrix
Number of 0s	Number of eigenvalues that are equal to 0 in normalized laplacian matrix
Number of 1s	Number of eigenvalues that are equal to 1 in normalized laplacian matrix
Number of 2s	Number of eigenvalues that are equal to 2 in normalized laplacian matrix
Lower slope	The slope of the line fitted for the eigenvalues of the normalized laplacian matrix that are between 0 and 1 when sorted
Upper slope	The slope of the line fitted for the eigenvalues of the normalized laplacian matrix that are between 1 and 2 when sorted
Normalized Laplacian Trace	Sum of the eigenvalues of normalized laplacian matrix
Normalized Laplacian Energy	Sum of the squares of eigenvalues of normalized laplacian matrix

Classification and Validation: Support vector machine (SVM) classification was employed for the classification of the two groups. Though alternate supervised learning techniques may also be utilized, as we shall see in the next section, SVM classifier yielded the highest classification accuracy among the other well known candidates. We used radial basis function, also referred to as Gaussian kernel, in the form of $K(\mathbf{x}_i, \mathbf{x}_j) = \exp(-\frac{|\mathbf{x}_i - \mathbf{x}_j|^2}{2\sigma^2})$ to transform the increase in the dimensionality of the data for better separability. We performed a parameter search to identify σ that achieves the highest classification accuracy. We sought σ in the set of candidate values that varied from 1.0 to 6.0 with 0.1 steps and determined that σ equaling 3.6 achieved the best performance in the identification of the patient's state.

The data is normalized so that the features have zero mean and unit variance to reduce the scale differences within different features. In order to obtain unbiased performance estimates, patient-based leave-one-out cross-validation was performed. The feature set was first divided into 32 disjoint partitions for each patients data. For each patient, a classifier was trained with the remaining 31 patients data and then tested on the retained data. The results for each patient were then combined to find the overall classification accuracy.

3 Results

We generated brain connectome networks as described previously for 32 patients each of which with four independent trackings. We then characterized the graphs using the 32 features described in Table 1 and using SVM classifier with RBF kernel we discriminated ASD patients from TD control with leave-one-patient-out cross-validation.

Given the large number of features, we performed feature selection based on *t-statistic* to identify the most discriminative features. For a given feature i, the t-statistic to test whether the population means are different is calculated as

$$t(i) = \frac{|\mu_1(i) - \mu_2(i)|}{\sqrt{\frac{\sigma_1^2(i)}{N_1} + \frac{\sigma_2^2(i)}{N_2}}} \tag{1}$$

where $\mu_k(i)$, $\sigma_k(i)$, and N_k are the sample mean, standard deviation, and size of the kth class ($k \in \{1, 2\}$) for ith feature, respectively. The features with high discriminative power get higher score. We tested the grading accuracy of the feature sets constituted by the first M most discriminative features. We varied M from 1 to 32, and report the grading accuracy in Fig. 2. It is seen that a classification accuracy of 86.72% can be achieved using the top four or five features. When we investigated the results of this case, it is seen that 9 out of 64 ASD trackings were identified as TD control and eight out of 64 TD control trackings were classified as ASD, and the rest of the trackings were classified accurately.

In order to compare our result to our earlier study that only considered the betweenness centrality of speech related locations in the brain [6], we also performed classification using the average betweenness centrality alone. Our result

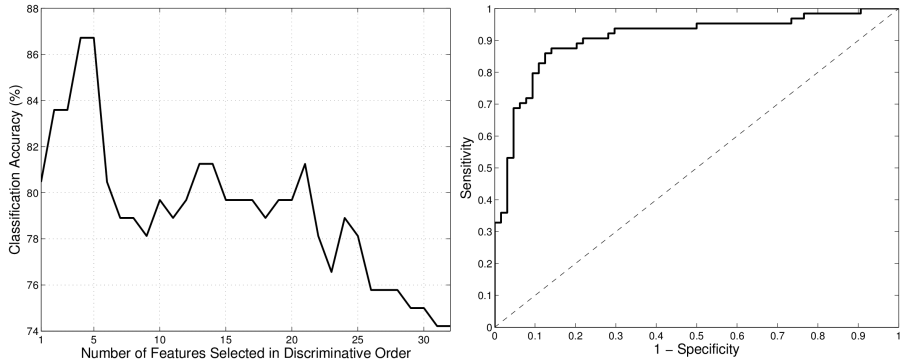

Fig. 2. Left: Influence of the number of discriminative features selected for classification on the classification accuracy. Highest grading accuracy achieved either the top four or five features selected. **Right:** Receiver operating characteristics for the SVM classifier with RBF kernel. The area under the curve is 0.9067.

showed 78.9% classification accuracy can be achieved using this feature alone. It is clear that considering additional features improved the classification accuracy significantly.

Independent of the learning method, we could achieve a consistent classification accuracy over 80%. Table 2 compares the classification accuracies of different classification methods. It is clear that SVM classifier achieves the highest overall accuracy in identifying the patient's neurological state. This is not unexpected as SVM classifiers are known to be highly successful in biomedical applications [18].

Table 2. Classification accuracy for different learning methods. SVM with RBF kernel yields the highest classification accuracy.

Learning Method	Classification Accuracy (%)
Support Vector Machines (RBF Kernel)	**86.72**
Support Vector Machines (Linear Kernel)	85.16
Linear Discriminant Analysis	84.38
Naïve Bayes Classifier	78.13
AdaBoost (Decision Stumps)	81.25

We then investigated how often a feature was in the top five of features for classification for a range of thresholds where the discriminative influence of each feature was given by t-statistic. Table 3 shows the frequency of discriminative features that appear in the top five feature for different thresholds. The Giant Connected Component Ratio was consistently a discriminative feature for every threshold in the range. For threshold $N = 26$, with the highest classification accuracy the top five features with the highest t-statistics were Clustering Coef-

ficient D, Giant Connected Component Ratio, Average Connected Component Size, Normalized Laplacian Trace, and Normalized Laplacian Energy.

Table 3. Histogram of highest discriminative features where the frequency shows the number of times the feature was in the top five discriminative features according to t-statistic for a link threshold (N) ranging from 14 to 30.

Feature	Frequency
Giant Connected Component Ratio	17
Clustering Coefficient D	16
Normalized Laplacian Trace	15
Average Connected Component Size	11
Normalized Laplacian Energy	10
Second Largest Eigenvalue Adjacency	7
Clustering Coefficient C	4
Average Betweenness Centrality	1

Finally, we give the receiver operating characteristics (ROC) to evaluate the performance of the classification. ROC curve plots the *sensitivity* against the $1-$*specificity* at different threshold settings. For the SVM classifier, we used the distance from the maximum-margin hyperplane as the decision threshold. Figure 2 shows the ROC curve for our classifier. The area under the curve (AUC) is 0.9067, which is considered as a well-discriminating classifier.

4 Discussion

We show that global connectome features are useful to divide a group into patients suffering from ASD and healthy controls with good accuracy. A range of features, which have been neglected in the literature so far can be a valuable tool in identifying changes in the structure of the connectome.

Our patients have been matched for IQ and as such provide a sample of ASD that is closest to a normal population and as such presents the most prominent challenge considering classification in the context of ASD. In this light, our classification results are surprisingly good. Thus, quantitative connectomics may provide a powerful tool to further the understanding of the functioning of the human brain, both under normal conditions as well as in disease.

Identification of the features of the connectome which are consistently and significantly affected in disease using the full power of network graph analysis is an important step in this direction.

References

1. Bullmore E, Sporns O. Complex brain networks: graph theoretical analysis of structural and functional systems. Nat Rev Neurosci. 2009 March;10:186–198.

2. Travers BG, Adluru N, Ennis C, Tromp DPM, Destiche D, Doran S, et al. Diffusion Tensor Imaging in Autism Spectrum Disorder: A Review. Autism Research. 2012;.
3. Lewis WW, Sahin M, Scherrer B, Peters JM, Suarez RO, Vogel-Farley VK, et al. Impaired Language Pathways in Tuberous Sclerosis Complex Patients with Autism Spectrum Disorders. Cerebral Cortex. 2012;.
4. Griffa A, Baumann PS, Thiran J-P, Hagmann P. Structural connectomics in brain diseases. NeuroImage. 2013;.
5. Li H, Xue Z, Ellmore TM, Frye RE, Wong STC. Network-based analysis reveals stronger local diffusion-based connectivity and different correlations with oral language skills in brains of children with high functioning autism spectrum disorders. Human Brain Mapping. 2012;.
6. Goch CJ, Stieltjes B, Henze R, Hering J, Meinzer HP, Fritzsche KH. Reduced centrality of Wernicke's area in autism. Proceedings of SPIE Medical Imaging 2013: Biomedical Applications in Molecular, Structural, and Functional Imaging. 2013; p. 867223–867223–6.
7. Demir C, Gultekin S, Yener B. Learning the topological properties of brain tumors. IEEE/ACM Transactions on Computational Biology and Bioinformatics **2**(3), 262–270 (2005);.
8. Bilgin C, Demir C, Nagi C, Yener B. Cell-graph mining for breast tissue modeling and classification. Proc. of 29th Annual International Conference of the IEEE Engineering in Medicine and Biology Society. 5311–5314, IEEE (2007);.
9. Bilgin C, Bullough P, Plopper G, Yener B. Ecm-aware cell-graph mining for bone tissue modeling and classification. Data mining and knowledge discovery **20**(3), 416–438 (2010);.
10. Oztan B, Shubert K, Bjornsson C, Plopper G, Yener B. Biologically-Driven Cell-Graphs for Breast Tissue Grading. Proc. of IEEE Symp. on Biomed. Imaging, 141–144 (2013);.
11. Lund AW, Bilgin CC, Hasan MA, McKeen LM, Stegemann JP, Yener B, Zaki MJ, Plopper GE. Quantification of spatial parameters in 3D cellular constructs using graph theory. Journal of Biomedicine and Biotechnology. (2009);.
12. Bilgin CC, Lund AW, Can A, Plopper GE, Yener B. Quantification of three-dimensional cell-mediated collagen remodeling using graph theory. PloS one **5**(9), (2010);.
13. Dhulekar N, Bange L, Baskaran A, Yuan D, Oztan B, Yener B, Ray S, Larsen M. A novel dynamic graph-based computational model for predicting salivary gland branching morphogenesis. Bioinformatics and Biomedicine (BIBM), 2012 IEEE International Conference on, 1–8 (2012);.
14. Fischl B, van der Kouwe A, Destrieux C, Halgren E, Ségonne F, Salat DH, et al. Automatically Parcellating the Human Cerebral Cortex. Cerebral Cortex. 2004;14(1):11–22.
15. Jenkinson M, Beckmann CF, Behrens TEJ, Woolrich MW, Smith SM. FSL. NeuroImage. 2012;62(2):782 – 790.
16. Fritzsche KH, Neher PF, Reicht I, van Bruggen T, Goch C, Reisert M, et al. MITK Diffusion Imaging. Methods of Information in Medicine. 2012;.
17. Neher PF, Stieltjes B, Reisert M, Reicht I, Meinzer HP, Fritzsche KH. MITK Global Tractography. SPIE Medical Imaging 2012: Image Processing. 2012;.
18. Yang ZR. Biological applications of support vector machines. Briefings in bioinformatics **5**(4), 328–338 (2004);.